An improved electrochemical model for the NH$_3$ fed proton conducting solid oxide fuel cells at intermediate temperatures

Meng Ni*, Dennis Y.C. Leung, Michael K.H. Leung

Department of Mechanical Engineering, The University of Hong Kong, Pokfulam Road, Hong Kong, PR China

ABSTRACT

An improved electrochemical model is developed to study the ammonia fed solid oxide fuel cell based on proton conducting electrolyte (SOFC-H). Including the chemical reaction kinetics of NH$_3$ catalytic thermal decomposition, the present model can be used to predict the performance of the NH$_3$ fed SOFC-H at an intermediate temperature (i.e. 773 K). Comparison between the simulation results using the present model and experimental data from literature validates the accuracy of this model. Parametrical analyses reveal that at a high operating temperature (i.e. 1073 K), the NH$_3$ fuel is completely decomposed to H$_2$ and N$_2$ within a very thin layer (30 μm) near the anode surface of an SOFC-H. It is also found that operating the NH$_3$ fed SOFC-H at an intermediate temperature of 773 K is feasible due to sufficiently high rate of NH$_3$ decomposition. However, further decreasing the temperature to 673 K is not recommended as less than 10% NH$_3$ fuel can be decomposed to H$_2$ and N$_2$ in the SOFC-H. The effects of current density and electrode microstructure on the performance of the NH$_3$ fed SOFC-H are also studied. It is found that increasing electrode porosity and pore size is beneficial to increase the partial pressure of H$_2$ at the anode–electrolyte interface. The model developed in this paper can be extended to 2D or 3D models to study practical tubular or planar SOFCs.

© 2008 Elsevier B.V. All rights reserved.

1. Introduction

Solid oxide fuel cells (SOFCs) have been identified as a promising power source for clean and efficient electricity generation [1]. One advantage of an SOFC is its fuel flexibility. As SOFCs work at a high temperature between 1073 K and 1273 K, various alternative fuels, such as hydrogen, bio-methanol, bio-ethanol and biogas can be directly used in an SOFC [2–6]. In recent years, ammonia (NH$_3$) emerges as a promising fuel for SOFCs because it is relatively cheap, easy to store and transport, and relatively safe due to any leakage being easily detectable by its pungent odor. In addition, the infrastructure of ammonia technology has been well established. Therefore, there is increasing interest in using ammonia in fuel cells, especially SOFCs [7–23].

Conventionally, an SOFC employs oxygen ion conducting ceramics as its electrolyte (SOFC-O), i.e. yttria-stabilized zirconia (YSZ). In order to achieve high performance, SOFCs are usually operated at a high temperature between 1073 K and 1273 K. At high temperatures, both electrochemical reactions and ion conduction are fast, which in turn results in low activation and ohmic over-

potentials. However, the high operating temperature limits the choice of materials used for SOFCs and also causes catalyst sintering and thermal expansion mismatch of SOFC components. In order to resolve these material and stability problems, a lot of research efforts have been made to operate the SOFC at intermediate temperatures. However, the ionic conductivity of YSZ decreases considerably with decreasing temperature, which can cause high ohmic loss at the electrolyte. For comparison, some proton conducting ceramics show good ionic conductivity at intermediate temperatures (673–773 K) and are thus suitable candidates for use as SOFC electrolyte. Therefore, there is increasing interest in SOFC using proton conducting electrolyte (SOFC-H). The most frequently used proton conducting electrolytes are BaCeO$_3$-based ceramics, such as BaCeO$_3$ doped with Gd, Nd, Sm or Y [14,15,21]. Compared with conventional SOFC-O, the SOFC-H is advantageous as complete fuel utilization can be easily achieved in an SOFC-H. In addition, when ammonia is used as a fuel, an SOFC-H has an additional advantage, as no harmful nitrogen oxide gas will be generated [7,8,20]. For comparison, nitrogen oxide may be formed in the anode chamber of an SOFC-O as oxygen ions transporting through the dense electrolyte may react with N$_2$ at the surface of the catalyst particles. Previous thermodynamic analyses have demonstrated that fed with hydrogen, methane, ethanol, or ammonia, the SOFC-H has a higher maximum energy efficiency than the SOFC-O [24–28]. However,

* Corresponding author. Tel.: +852 2859 2811; fax: +852 2858 5415.
E-mail addresses: memni@graduate.hku.hk, mengni@hku.hk (M. Ni).

the above-mentioned thermodynamic studies only consider the Nernst potentials of SOFC-O and SOFC-H while the overpotentials are not included. In a recent publication, a simplified electrochemical model has been developed to predict the actual performance of ammonia fed SOFC-H [29]. The model considers all overpotentials involved in SOFC-H operation but assumes complete decomposition of NH_3 at the anode surface. This assumption greatly simplifies the model as the catalytic thermal decomposition of NH_3 and multi-component mass transfer phenomena in the porous anode can be determined separately. However, this assumption is only valid for SOFC-H working at a high temperature (i.e. 1073 K) and may become invalid for SOFC-H working at an intermediate temperature (i.e. 773 K). In this study, an improved electrochemical model is developed to study the performance of the NH_3 fed SOFC-H at an intermediate temperature. The coupled mass transfer and chemical reaction in the porous anode are fully considered in this model.

2. Electrochemical model

2.1. Working mechanisms of the NH_3 fed SOFC-H

The working mechanisms of the NH_3 fed SOFC-H are shown in Fig. 1. At the anode, NH_3 undergoes catalytic thermal decomposition over a Ni catalyst as

$$2NH_3 \rightarrow N_2 + 3H_2 \tag{1}$$

The N_2 is removed from the anode chamber by the gas stream, while the H_2 produced undergoes electrochemical reactions at the anode–electrolyte interface to produce protons and electrons. The electrons traveling from the anode to the cathode through an external circuit yield an electrical power output. The protons are transported through the dense electrolyte to the cathode chamber and undergo electrochemical reactions with oxygen molecules and electrons to form H_2O at the cathode–electrolyte interface.

2.2. Working potential of the NH_3 fed SOFC-H

Considering all the overpotentials in the NH_3 fed SOFC-H, the external voltage (V) can be expressed as

$$V = E - \eta_{act,a} - \eta_{act,c} - \eta_{ohm} \tag{2}$$

$$E = E_0 + \frac{RT}{2F} \ln \left(\frac{P_{H_2,a}^{Int}(P_{O_2,c}^{Int})^{0.5}}{P_{H_2O,c}^{Int}} \right) \tag{3}$$

where E_0 is the ideal standard potential of the SOFC-H, which can be obtained from literature [30,31]; E is the reversible (equilibrium) potential, R is the ideal gas constant; T is the operating temper-
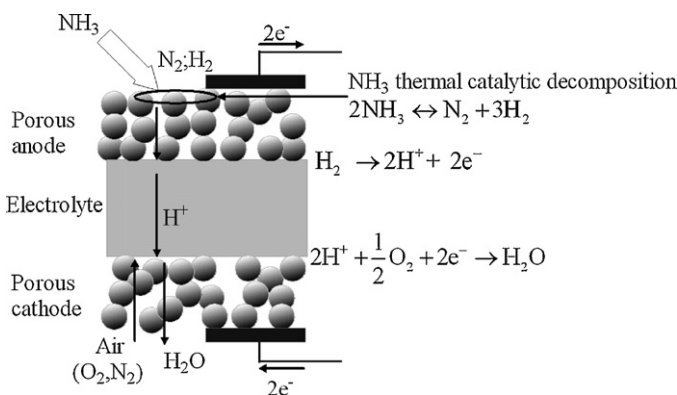
ature; F is the Faraday constant; $P_{H_2,a}$, $P_{H_2O,c}$ and $P_{O_2,c}$ are the partial pressure of H_2 (anode), H_2O (cathode), and O_2 (cathode), respectively. The superscript 'Int' refers to the electrode–electrolyte interface. $\eta_{act,a}$ and $\eta_{act,c}$ are the activation overpotentials at the anode and cathode, respectively, which can be calculated with the Butler–Volmer equation [31]. η_{ohm} is the ohmic overpotential at the electrolyte and can be analytically calculated with Ohm's law [31]. It should be mentioned that the concentration overpotentials are implicitly included in the reversible potential (E), since the partial pressures of gaseous species used in Eq. (3) are evaluated at the electrode–electrolyte interface [32]. In order to obtain these interfacial partial pressures, the characteristics of mass transport and chemical/electrochemical reactions in the porous electrodes must be obtained.

2.3. Reaction and mass transport in porous electrode

2.3.1. Anode

In literature, there are a lot of research works on thermal decomposition of ammonia with different catalysts. Many metals and compounds, such as Fe, Ni, Pt, Ru, Ir, Pd, Ni–Pt, Ni/Ru, etc. have been examined for ammonia thermal decomposition [33–42]. In most of these studies, dilute ammonia gas (at ppm level) was used for investigation. Possible reaction steps are: (1) adsorption of NH_3 on catalyst surface; (2) cleavage of N–H bond of adsorbed NH_3; and (3) recombinative desorption of nitrogen atoms [37]. Although there is no consensus on the rate limiting steps of NH_3 decomposition on different catalyst and under different operating conditions, it was normally observed that the rate of ammonia thermal decomposition is inhibited by hydrogen partial pressure at a relatively low temperature (below 673 K) and low partial pressure of NH_3 (ppm level). Based on experimental observation, Bradford et al. [33] found that the rate of NH_3 decomposition followed the equation:

$$r = kP_{NH_3}^{\alpha} P_{H_2}^{\beta} \tag{4}$$

where α varied from 0.69 to 0.75; β varied from −1.5 to −2.0; and k is a constant for Eq. (4). The reported activation energy was about 23 kcal mol^{-1}. This above equation reveals the strong inhibition effect of hydrogen partial pressure on the thermal decomposition of dilute NH_3 (ppm level) at a temperature of below 673 K. In a recent study of NH_3 thermal decomposition at a temperature of between 623 K and 923 K and a NH_3 partial pressure between 0.5 kPa and 2.0 kPa, the reaction rate of NH_3 decomposition over Ru based catalyst was found to satisfy the following equation [34]:

$$r = kP_{NH_3}^{\alpha} \tag{5}$$

where α was about 2.0, indicating that the reaction rate was second order with respect to NH_3 partial pressure. The second order dependence on NH_3 partial pressure was explained by the assumption that the recombinative desorption of nitrogen atoms was the rate-determining step [34,35].

The above results are applicable to dilute NH_3 at a ppm level. Chellappa et al. [36] investigated the decomposition kinetics of pure ammonia over Ni–Pt/Al$_2$O$_3$. They found that the decomposition kinetics of pure ammonia was quite different from those reported previously with diluted ammonia at a ppm level. At a temperature between 793 K and 963 K, the reaction rate was found first order with respect to NH_3 partial pressure (Eq. (6)) and no H_2 inhibition effect was observed. In addition, the activation energy (E_a) was found to be about 46.9 kcal mol^{-1} (equivalent to 196.2 kJ mol^{-1}).

$$r = k_0 \exp \left(-\frac{E_a}{RT} \right) P_{NH_3} \tag{6}$$

Obviously, the concentration of NH_3 in the NH_3 fed fuel cells should be high (much higher than the ppm level), thus the first

Fig. 1. Working mechanisms of the NH_3 fed SOFC-H.

order dependence of reaction rate on partial pressure of NH_3 was adopted in this research. The inhibition effect of H_2 partial pressure is assumed to be negligible as it is significant only at low temperature and very low NH_3 concentration [37]. Recently, Liu et al. [38] investigated the decomposition kinetics of NH_3 over nano-sized Ni/SBA-15 (SBA: Santa Barbara Amorphous) catalysts. The rate of H_2 formation (mmol min^{-1} g$_{cat}^{-1}$) increased from about 8.0 at 723 K to about 33 at 923 K. At a typical temperature of 773 K, the H_2 formation rate was about 17.5 mmol min^{-1} g$_{cat}^{-1}$. The pore volume of the Ni/SBA based catalysts ranged from 0.36 cm^3 g^{-1} to 0.82 cm^3 g^{-1}. In another recent study conducted by Zheng et al. [39], the kinetics of NH_3 decomposition to H_2 over Ni/Al$_2$O$_3$ catalysts have been investigated. It was reported that at a temperature of 773 K, the rate of H_2 formation was about 24.1 mmol min^{-1} g$_{cat}^{-1}$. The pore volume of the Ni/Al$_2$O$_3$ based catalysts was found to be about 0.3 cm^3 g^{-1}. Assuming a porosity of 30%, the volume of the porous catalyst was about 1.0 cm^3 g^{-1}. In addition, other investigators also reported that the rate of hydrogen formation was about 20 mmol min^{-1} g$_{cat}^{-1}$ at a temperature of 773 K [40–42]. Adopting this hydrogen formation rate at 773 K, the coefficient k_0 can thus be determined (4.0×10^{15}) from Eq. (6). The rate of NH_3 decomposition can thus be expressed as

$$r = 4.0 \times 10^{15} \exp\left(-\frac{196,200.0}{RT}\right) P_{NH_3} \tag{7}$$

In a steady state, the transport of each participating component is determined by the local conservation of mass:

$$\frac{dN_{NH_3}}{dx} = -r \tag{8}$$

$$\frac{dN_{H_2}}{dx} = 1.5r \tag{9}$$

$$\frac{dN_{N_2,a}}{dx} = 0.5r \tag{10}$$

where N_i is the flux of species i (mol m^{-2} s^{-1}); x is the depth measured from the electrode surface. The subscript 'a' refers to the anode.

The dusty gas model (DGM) is used to model the multi-component mass transfer within the anode and cathode as it can predict the mass transfer in porous media more accurately than the Fick's model and Stefan–Maxwell model [43,44]. According to DGM, the transport of gas species in both anode and cathode is governed by

$$\frac{N_i}{D_{i,k}^{eff}} + \sum_{j=1, j \neq i}^{n} \frac{y_j N_i - y_i N_j}{D_{ij}^{eff}} = -\frac{1}{RT}\left[P\frac{dy_i}{dx} + y_i \frac{dP}{dx}\left(1 + \frac{B_0 P}{D_{i,k}^{eff}\mu}\right)\right] \tag{11}$$

where N_i is the flux of gas species i; y_i is the molar fraction of gas species i; $D_{i,k}^{eff}$ is the effective Knudsen diffusion coefficient of species i; D_{ij}^{eff} is the effective binary molecular diffusion coefficient of species i and j; μ is the viscosity of the gas mixture; and B_0 is the permeability of the porous electrode, which can be calculated by the Kozeny–Carman relationship [44]:

$$B_0 = \frac{\varepsilon^3}{72\xi(1-\varepsilon)^2}(2r_p)^2 \tag{12}$$

The effective diffusion coefficients ($D_{i,k}^{eff}$, D_{ij}^{eff}) can be determined by the following equations [45–47]:

$$D_{i,k}^{eff} = \frac{\varepsilon}{\xi}\frac{4r_p}{3}\sqrt{\frac{8RT}{\pi M_i}} \tag{13}$$

$$D_{ij}^{eff} = 0.00133\frac{\varepsilon}{\xi}\left(\frac{1}{M_i} + \frac{1}{M_j}\right)^{0.5}\frac{T^{1.5}}{P\sigma_{i,j}^2\Omega_D} \tag{14}$$

where ε, ξ, and r_p are the porosity, tortuosity and mean pore radius of the electrodes; M_i is the molecular weight of species i; Ω_D a dimensionless diffusion collision integral; and $\sigma_{i,j}$ is the mean characteristic length of species i and j. The values of Ω_D and $\sigma_{i,j}$ can be obtained from the literature [48].

The pressure gradient (dP/dx) can be evaluated with a method developed by Zhu and Kee [49]:

$$\frac{dP}{dx} = -\frac{\sum_{i=1}^{n}(N_i/D_{i,k}^{eff})}{(1/RT) + (B_0 P/RT\mu)\sum_{i=1}^{n}(y_i/D_{i,k}^{eff})} \tag{15}$$

At the anode surface, the molar fractions of each species are known. At the electrode–electrolyte interface, electrochemical reactions take place and thus the flux of H_2 can be related with the current density as

$$N_{H_2}\big|_{x=d_a} = \frac{J}{2F} \tag{16}$$

where J is the current density (A m^{-2}) and d_a is the thickness of the anode. As the remaining species are not involved in the electrochemical reaction, their fluxes at the electrode–electrolyte interface are equal to zero.

$$\left(N_{NH_3}\big|_{x=d_a} = 0 \quad \text{and} \quad N_{N_2,a}\big|_{x=d_a} = 0\right)$$

The above governing equations (Eqs. (7)–(15)) are inter-related differential equations and can be solved by numerical method. Finite difference method was used to discretize the governing equations. An iterative scheme was developed to obtain the solution at the discrete grids. Calculations were repeated till convergence was achieved. Solving the above-mentioned equations, the partial pressure of H_2 at the anode–electrolyte interface can thus be obtained.

2.3.2. Cathode

In the cathode, O_2 is electrochemically consumed while H_2O is electrochemically produced and no chemical reaction is involved. Therefore, the transport of gas species (O_2, N_2 and H_2O) can be determined by

$$\frac{dN_i}{dx} = 0 \quad (i = O_2, N_2 \text{ and } H_2O) \tag{17}$$

The fluxes of the transporting species can be determined by the DGM (Eq. (11)). Similar to the anode, the molar fractions of gas species at the cathode surface are given. At the cathode–electrolyte interface, the fluxes of O_2 and H_2O can be related with the current density as

$$N_{O_2}\big|_{x=d_c} = \frac{J}{4F} \tag{18}$$

$$N_{H_2O}\big|_{x=d_c} = -\frac{J}{2F} \tag{19}$$

After solving the governing equation (Eqs. (11) and (15)) with the above boundary conditions, the partial pressures of O_2 and H_2O at the cathode–electrolyte can thus be obtained. After obtaining the partial pressures of electrochemical reaction species (H_2, H_2O and O_2) at the electrode–electrolyte interface, the equilibrium potential of the NH_3 fed SOFC-H can thus be calculated with Eq. (3).

Table 1
Input parameters for the present electrochemical model of the NH_3 fed SOFC-H

Parameter	Value
Operating temperature, T (K)	1073, 873, 773, 673
Operating pressure, P (atm)	1.0
Gas composition at the electrode surface (%)	
Anode: NH_3	100
Cathode: $H_2O/O_2/N_2$	3/18/79
Exchange current density of anode ($A m^{-2}$)	5300.0 [30,31]
Exchange current density of cathode ($A m^{-2}$)	2000.0 [30,31]
Electrode porosity	0.4 [45]
Electrode tortuosity	5.0 [45]
Electrode pore radius (μm)	0.5 [45]
Conductivity of electrolyte (i.e. Sm-doped $BaCeO_3$) at 1073 K	$0.94 S m^{-1}$ (estimated from [50])
Component thickness (μm)	
Electrolyte	50.0
Anode	500.0
Cathode	50.0

3. Results and discussion

3.1. Model evaluation

In the literature, there are very few experimental data available on the NH_3 fed SOFC-H. In this section, an evaluation of the model was conducted by comparing the present modeling results with the experimental data from literature [8]. In the experiment, the Gd-doped $BaCeO_3$ (BCGO) electrolyte was prepared by a modified glycine-nitrate process with stoichiometric precursors of $Ba(CH_3COO)_2$, $Ce(NO_3)_2$ and $Gd(NO_3)_2$. The composite anode substrate and the BCGO electrolyte film were fabricated by the dry-pressing method. The SOFC-H was based on anode-supported configuration, in which the thickness of anode and electrolyte were 650 μm and 50 μm, respectively. Commercial industrial grade ammonia and humid oxygen (3% H_2O) was used as the fuel and oxidant, respectively. The tests were conducted at a typical temperature of 973 K and a pressure of 1.0 atm. The values of input parameters, such as porosity, pore radius, and tortuosity, are summarized in Table 1. As can be seen from Fig. 2, the present simulation results agreed reasonably well with the experimental data. Therefore, the model developed in this paper is reliable for the following parametrical analyses.
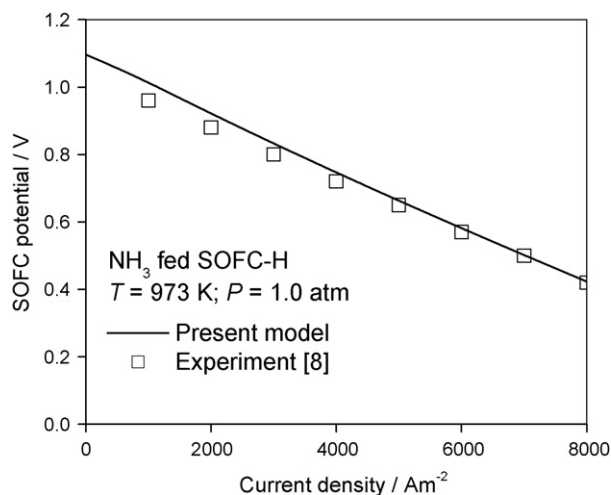

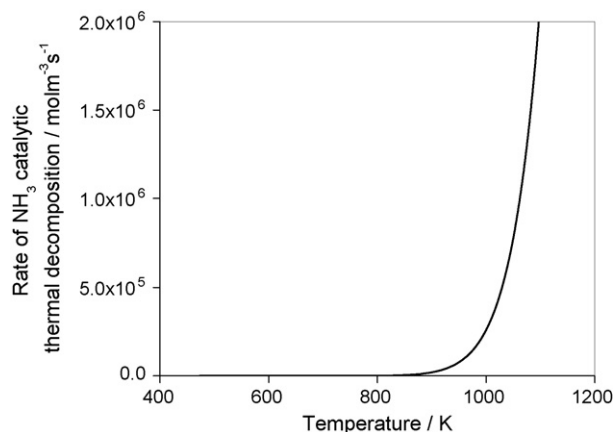**Fig. 2.** Comparison between simulation results with experimental data from literature for model validation.

Fig. 3. Dependence of NH_3 decomposition rate on temperature.

3.2. Temperature effect

Temperature is an important parameter governing the performance of the NH_3 fed SOFC-H. In this section, the effects of temperature on the NH_3 catalytic thermal decomposition kinetics and the SOFC-H performance are investigated.

Fig. 3 shows the temperature dependence of NH_3 catalytic thermal decomposition at a NH_3 pressure of 1.0 atm. As can be seen, the rate of NH_3 thermal decomposition strongly depends on temperature, i.e. the reaction rate increases significantly from about $1.0 mol m^{-3} s^{-1}$ at a temperature of 673 K to $3.6 \times 10^7 mol m^{-3} s^{-1}$ at a temperature of 1273 K. This is consistent with the experimental observations in literature [36,37].

The distributions of NH_3 catalytic thermal decomposition rate in the porous anode of an SOFC-H at various temperatures are shown in Fig. 4(a)–(d). For SOFC-H operated at a high temperature (1073 K or 873 K), the rate of NH_3 catalytic thermal decomposition is high and the NH_3 fuel can be completely decomposed before reaching the anode–electrolyte interface (Fig. 4(a), (b), and (e)). Especially at a temperature of 1073 K, the rate of NH_3 decomposition decreases very quickly from about $4.0 \times 10^5 mol m^{-3} s^{-1}$ to $0.0 mol m^{-3} s^{-1}$ within a very thin layer (about 30 μm) near the anode surface (Fig. 4(a)). This is because the rate of NH_3 decomposition is so high that the NH_3 fuel is completely decomposed to H_2 and N_2 in a thin layer of the anode surface (Fig. 4(e)). In an experimental investigation of the NH_3 fed SOFC-H at a temperature of 1073 K, Zhang et al. observed that NH_3 was decomposed to H_2 and N_2 before reaching the anode–electrolyte interface [18]. Therefore, the present finding agrees with the experimental observations in literature. In our previous electrochemical model of the NH_3 fed SOFC-H working at a temperature of 1073 K, we assume that NH_3 is completely decomposed near the anode surface [29]. The finding of this study justifies the assumption made in our previous study. When the SOFC-H is operated at a lower temperature (i.e. 773 K or 673 K), the rate of NH_3 decomposition is lower and only part of the NH_3 fuel can be decomposed to H_2 and N_2 in the SOFC-H (Fig. 4(c)–(e)). At a temperature of 673 K, less than 10% NH_3 fuel can be decomposed throughout the anode of SOFC-H because of too low NH_3 decomposition kinetics (Fig. 4(d) and (e)). From experiments, it is known that the performance of the NH_3 fed SOFC-H is highly dependent on the extent of NH_3 decomposition in the SOFC-H [8,9,11]. Therefore, it can be seen from the present study that a too low temperature (i.e. 673 K) is not feasible for the NH_3 fed SOFC-H, unless very active catalyst for NH_3 decomposition can be developed. On the other hand, a considerable amount of NH_3 can be decomposed to H_2 and N_2 at a temperature of 773 K in the SOFC-H, although the conversion is not 100% (Fig. 4(c)
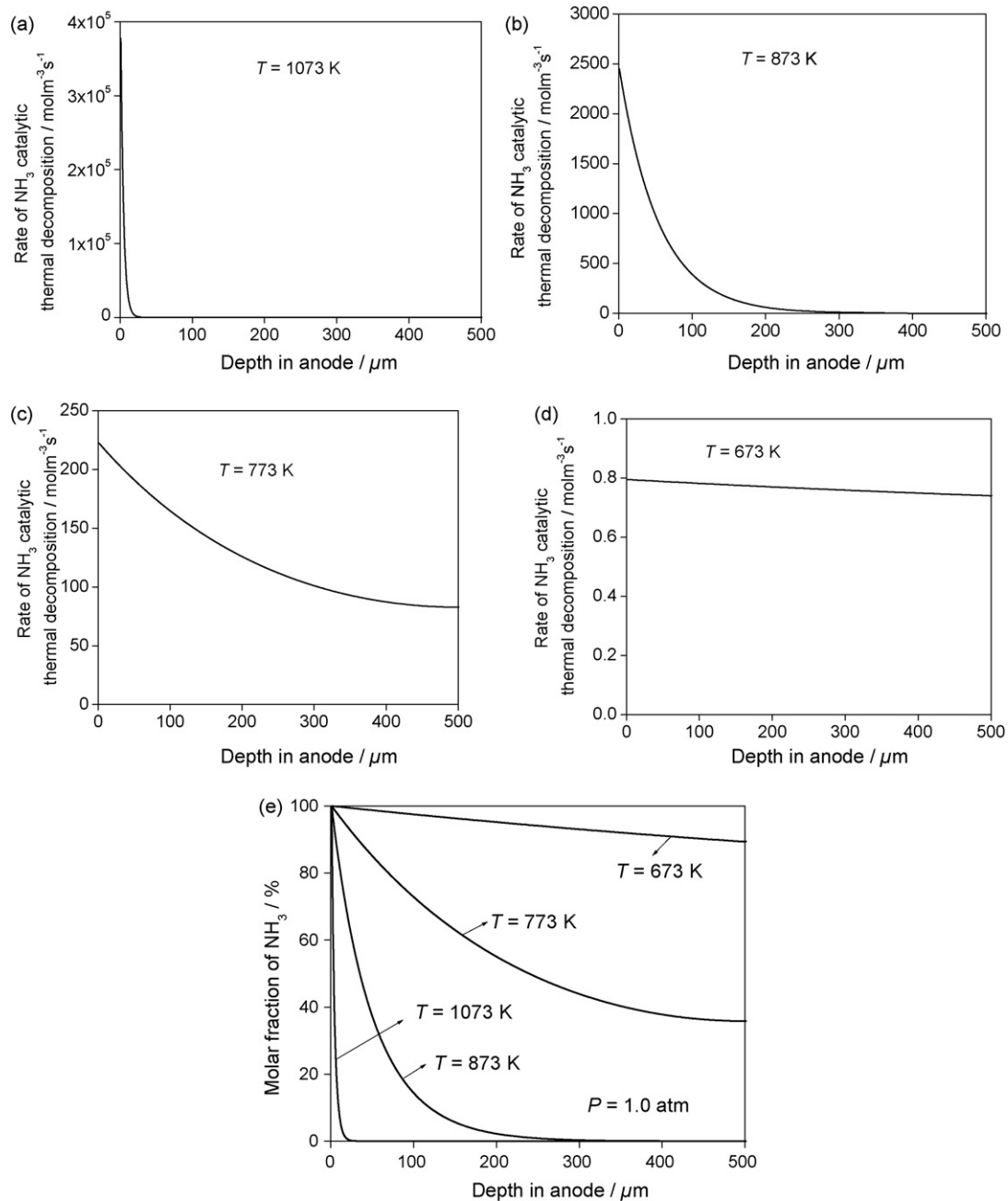
Fig. 4. Effect of operating temperature on the performance of the NH₃ fed SOFC-H: (a) NH₃ decomposition rate at 1073 K; (b) NH₃ decomposition rate at 873 K; (c) NH₃ decomposition rate at 773 K; (d) NH₃ decomposition rate at 673 K; and (e) molar fraction of NH₃.

and (e)). Therefore, it is possible to operate the NH₃ fed SOFC-H at a temperature of 773 K with acceptable cell performance. In Ma's study, it is reported that 100% NH₃ decomposition is achievable for SOFC-H working at a temperature of 873 K while the decomposition of NH₃ is incomplete when the temperature is reduced to 773 K [9]. In another study conducted by Maffei et al. [17], it is found that the NH₃ conversion is close to 100% at a temperature of 873 K, while it is about 30–55% at a temperature of 773 K. The present modeling results are consistent with experimental data in literature.

In the following analyses, the temperature of 773 K is selected as a typical intermediate-temperature for the NH₃ fed SOFC-H. For any fuel fed SOFC-H, the porous cathode involves the same electrochemical reaction and mass transport phenomena, i.e. O₂ is consumed while H₂O is electrochemically produced at the porous

cathode. As the SOFC-H fed with H₂ and CH₄ has been investigated in our previous studies [45,51], the following sections will be focused on the chemical reaction and mass transport in the porous anode of the NH₃ fed SOFC-H.

3.3. Current density effect

Fig. 5 shows the effect of current density on the NH₃ decomposition kinetics and the SOFC-H performance at the typical temperature of 773 K. The pressure distribution in the porous anode of the NH₃ fed SOFC-H is shown in Fig. 5(a). At a low current density (i.e. 2000 A m⁻²), the anode pressure initially increases with increasing anode depth, and, after reaching a maximum, decreases slightly with further increasing anode depth (Fig. 5(a)).
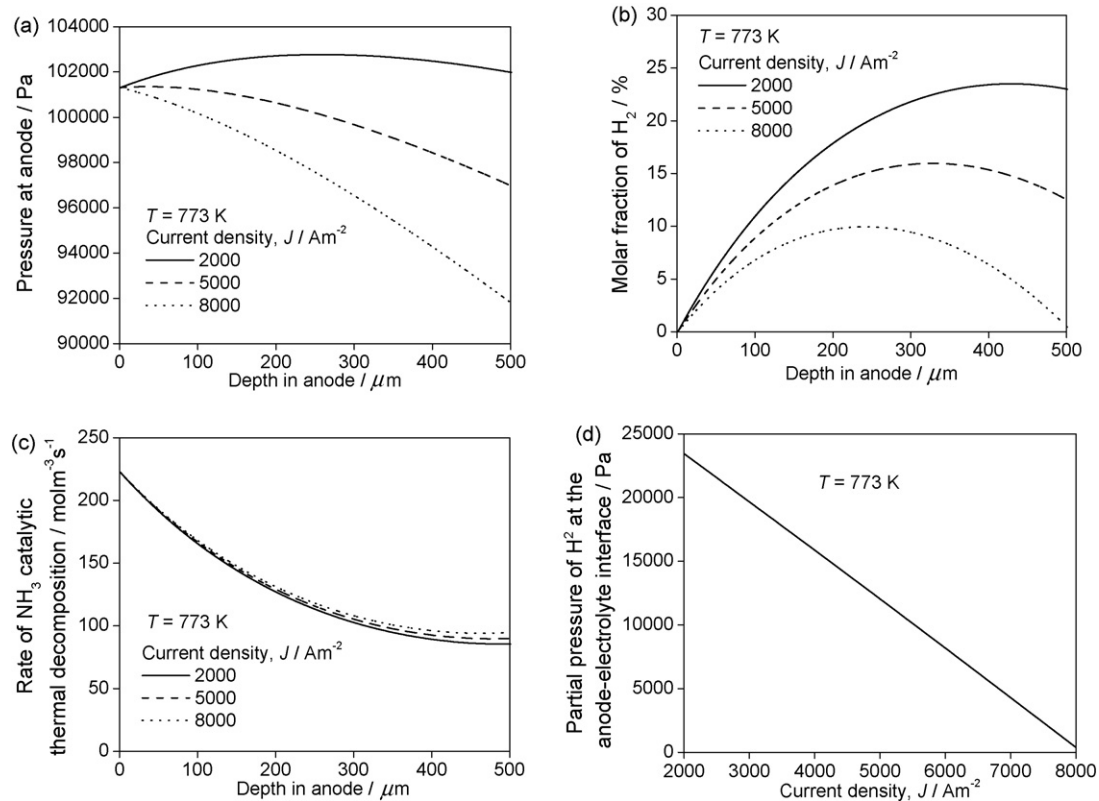
Fig. 5. Current density effect: (a) pressure in the anode; (b) molar fraction of H_2 in the anode; (c) rate of NH_3 decomposition; and (d) partial pressure of H_2 at the anode–electrolyte interface.

The molar fraction of H_2 shows a similar dependence on the anode depth (Fig. 5(b)). There are two mechanisms governing the pressure in the anode: (1) decomposition of NH_3 to H_2 and N_2, which tends to increase the pressure and (2) consumption of H_2 at the anode–electrolyte interface due to electrochemical reactions (H_2O is electrochemically produced at the cathode), which tends to reduce the pressure in the anode. At the surface of the anode, the decomposition of NH_3 is important due to a high partial pressure of NH_3. Therefore, the pressure increases with increasing anode depth near the anode surface. With an increase in anode depth, the rate of NH_3 decreases due to a lower partial pressure of NH_3 (multiplication of the anode pressure and the NH_3 molar fraction) (Fig. 5(c)). Thus, the pressure tends to decrease in a deeper layer because the resistance of the porous structure to the transport of gaseous species is relatively more important (Fig. 5(a)). At higher current densities (i.e. $5000\,A\,m^{-2}$ or $8000\,A\,m^{-2}$), the anode pressure decreases monotonically with increasing anode depth, indicating that the transporting resistance is the dominating mechanisms governing the anode pressure. Obviously, the molar fraction of H_2 decreases with increasing current density (Fig. 5(b)), which in turn results in a higher molar fraction of NH_3. The combined effect of higher NH_3 molar fraction and lower anode pressure at higher current density leads to a slightly higher NH_3 decomposition rate at a higher current density (Fig. 5(c)). In quantifying the electrochemical performance of an SOFC, the partial pressure of H_2 at the anode–electrolyte interface is often an important parameter, as it is directly related to the working potential of an SOFC. As both the anode pressure and the H_2 molar fraction decrease with increasing current density, the partial pressure of H_2 at the anode–electrolyte interface is found to decrease with increasing current density (Fig. 5(d)), which is consistent with previous analysis on SOFC-O and SOFC-H [29,31,45].

3.4. Micro-structural effect

In addition to the above-mentioned operating parameters (temperature and current density), the electrode microstructures also significantly influence the performance of SOFC-H. In this section, the effect of electrode microstructures on the NH_3 fed SOFC-H is investigated at a typical current density of $5000\,A\,m^{-2}$ and a typical temperature of 773 K. Electrode porosity and pore radius are studied due to their influences in SOFC performance.

Fig. 6(a) shows the distribution of pressure in the porous anode with varying electrode porosities. The anode pressure is found to increase with an increase in electrode porosity. This is because the diffusion coefficients (Eqs. (13) and (14)) are higher at a higher electrode porosity. In addition, the H_2 molar fraction is slightly higher at a higher electrode porosity, which in turn causes the NH_3 molar fraction to decrease slightly with increasing electrode porosity. As the anode pressure increases considerably with increasing electrode porosity and the reduction in NH_3 molar fraction is insignificant, the rate of NH_3 decomposition is found higher at a higher electrode porosity (Fig. 6(b)). Due to the slight increase in H_2 molar fraction and a considerable increase in the anode pressure, the partial pressure of H_2 at the anode–electrolyte interface increases with increasing electrode porosity (Fig. 6(c)). The effect of electrode pore radius on the anode pressure of the NH_3 fed SOFC-H is shown in Fig. 6(d). Similar to the electrode porosity, the anode pressure increases with increasing electrode pore radius due to higher diffusion coefficients (Eqs. (13) and (14)) and a lower transport resistance. The rate of NH_3 decomposition also increases with increasing electrode pore radius due to enhanced partial pressure of NH_3 (Fig. 6(e)). In addition, the partial pressure of H_2 at the anode–electrolyte interface initially increases considerably with increasing electrode pore radius and
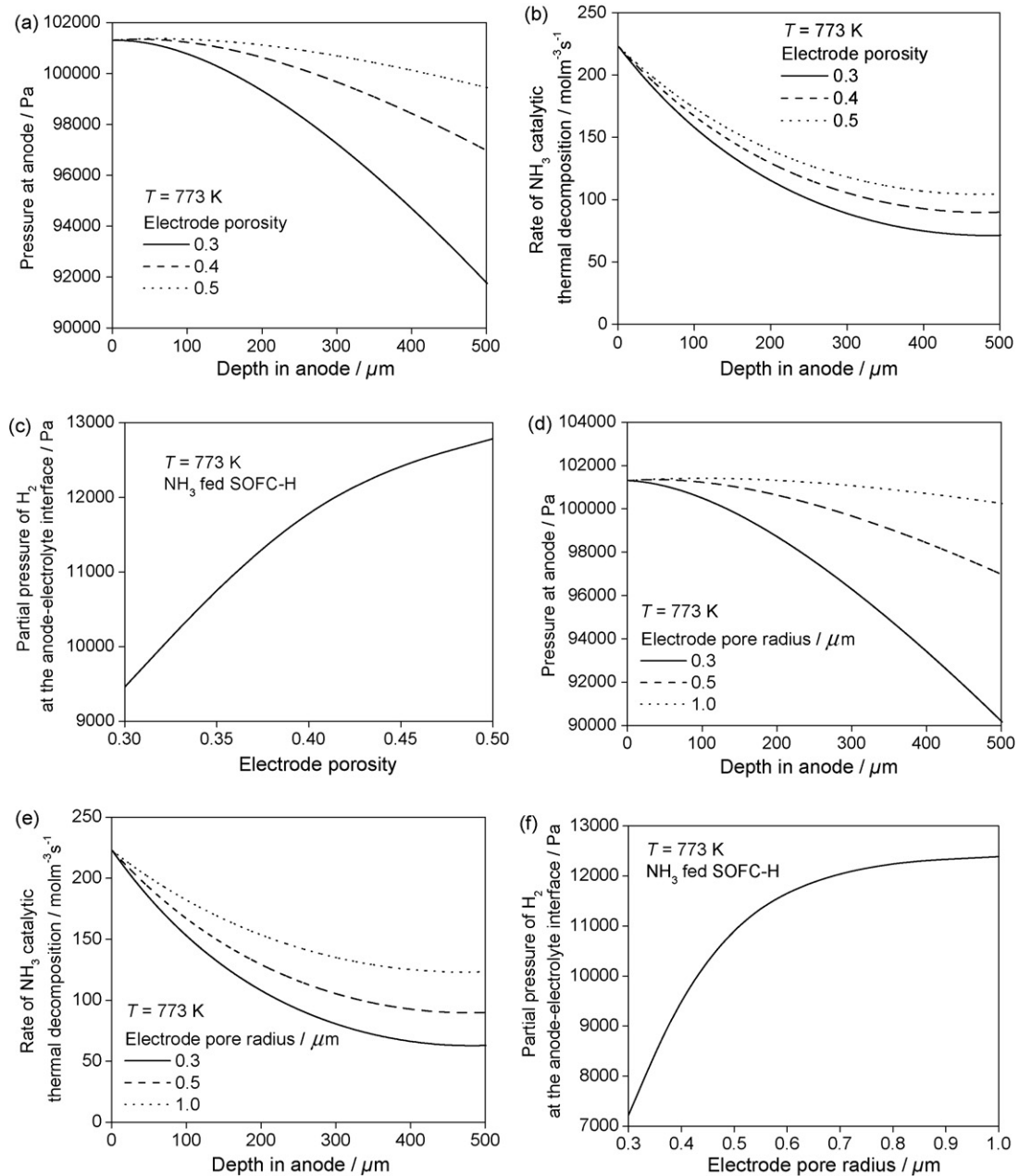
Fig. 6. Micro-structural effect: (a) effect of electrode porosity on anode pressure; (b) effect of electrode porosity on NH$_3$ decomposition rate; (c) effect of electrode porosity on partial pressure of H$_2$ at the anode–electrolyte interface; (d) effect of electrode pore radius on anode pressure; (e) effect of electrode pore radius on NH$_3$ decomposition rate; and (f) effect of electrode pore radius on partial pressure of H$_2$ at the anode–electrolyte interface.

then tends to level off when the electrode pore radius is higher than 0.6 μm (Fig. 6(f)). This is because at an electrode pore radius higher than 0.6 μm, both H$_2$ molar fraction and the anode pressure only slightly increase with a further increase in electrode pore radius.

4. Conclusion

An improved electrochemical model was developed to study the performance of the NH$_3$ fed SOFC-H. This model is an extension of our previous model assuming complete decomposition of NH$_3$ at the anode surface. Including the kinetics of NH$_3$ catalytic thermal decomposition, the present model is capable of predicting the performance of the NH$_3$ fed SOFC-H at intermediate temperatures

(i.e. 773 K). The simulation results are compared with experimental data from literature and good agreement is found between them, thus the model presented in this paper is validated.

Parametrical simulations are performed to study in detail the performance of the NH$_3$ fed SOFC-H. It is found that the NH$_3$ catalytic decomposition is highly temperature-dependent. At a temperature of 1073 K, the NH$_3$ fuel can be completely decomposed within a very thin layer (30 μm) near the anode surface. With a decrease in operating temperature, the rate of NH$_3$ catalytic thermal decomposition decreases considerably. It is found that it is feasible to operate the NH$_3$ fed SOFC-H at an intermediate temperature of 773 K, however, further reduction of the temperature to 673 K will dramatically decrease the SOFC-H performance as less than 10% NH$_3$ can be decomposed to H$_2$ and N$_2$.

Increasing current density slightly increases the rate of NH_3 decomposition but considerably decreases the partial pressure of H_2 at the anode–electrolyte interface. In addition, increased electrode porosity and pore size are both found beneficial to increase the partial pressure of H_2 at the anode–electrolyte interface.

The result of this study justifies the assumption made in our previous publication assuming complete NH_3 decomposition at the surface of SOFC-H anode. The model developed in this paper can be used to predict the performance of the NH_3 fed SOFC-H for design optimization.

Acknowledgements

References

[1] S.C. Singhal, K. Kendall, High Temperature Solid Oxide Fuel Cells: Fundamentals, Design, and Applications, Elsevier, Oxford; New York, 2003.
[2] W. Jamsak, S. Assabumrungrat, P.L. Douglas, E. Croiset, N. Laosiripojana, R. Suwanwarangkul, S. Charojrochkul, J. Power Sources 174 (2007) 191–198.
[3] H. Kronemayer, D. Barzan, M. Horiuchi, S. Suganuma, Y. Tokutake, C. Schulz, W.G. Bessler, J. Power Sources 166 (2007) 120–126.
[4] H.Y. Zhu, A.M. Colclasure, R.J. Kee, Y.B. Lin, S.A. Barnett, J. Power Sources 161 (2006) 413–419.
[5] G.K. Gupta, A.M. Dean, K. Ahn, R.J. Gorte, J. Power Sources 158 (2006) 497–503.
[6] J. Staniforth, K. Kendall, J. Power Sources 71 (1998) 275–277.
[7] A. Wojcik, H. Middleton, I. Damopoulos, J. Van Herle, J. Power Sources 118 (2003) 342–348.
[8] Q.L. Ma, R.R. Peng, Y.J. Lin, J.F. Gao, G.Y. Meng, J. Power Sources 161 (2006) 95–98.
[9] Q.L. Ma, R.R. Peng, L.Z. Tian, G.Y. Meng, Electrochem. Commun. 8 (2006) 1791–1795.
[10] G.G.M. Fournier, I.W. Cumming, K. Hellgardt, J. Power Sources 162 (2006) 198–206.
[11] Q.L. Ma, J.J. Ma, S. Zhou, R.Q. Yan, J.F. Gao, G.Y. Meng, J. Power Sources 164 (2007) 86–89.
[12] N.J.J. Dekker, G. Rietveld, J. Fuel Cell Sci. Technol. 3 (2006) 499–502.
[13] N. Maffei, L. Pelletier, J.P. Charland, A. McFarlan, J. Power Sources 162 (2006) 165–167.
[14] L. Pelletier, A. McFarlan, N. Maffei, J. Power Sources 145 (2005) 262–265.
[15] N. Maffei, L. Pelletier, J.P. Charland, A. McFarlan, J. Power Sources 140 (2005) 264–267.
[16] N. Maffei, L. Pelletier, J.P. Charland, A. McFarlan, Fuel Cells 7 (2007) 323–328.
[17] N. Maffei, L. Pelletier, A. McFarlan, J. Power Sources 175 (2008) 221–225.
[18] L. Zhang, Y. Cong, W. Yang, L. Lin, Chin. J. Catal. 28 (2007) 749–751.
[19] G.Y. Meng, C.R. Jiang, J.J. Ma, Q.L. Ma, X.Q. Liu, J. Power Sources 173 (2007) 189–193.
[20] L. Zhang, W. Yang, J. Power Sources 179 (2008) 92–95.
[21] K. Xie, Q.L. Ma, B. Lin, Y.Z. Jiang, J.F. Gao, X.Q. Liu, G.Y. Meng, J. Power Sources 170 (2007) 38–41.
[22] A. McFarlan, L. Pelletier, N. Maffei, J. Electrochem. Soc. 151 (2004) A930–932.
[23] J. Staniforth, R.M. Ormerod, Green Chem. 5 (2003) 606–609.
[24] M. Ni, D.Y.C. Leung, M.K.H. Leung, J. Power Sources 183 (2008) 682–686.
[25] A. Demin, P. Tsiakaras, Int. J. Hydrogen Energy 26 (2001) 1103–1108.
[26] A.K. Demin, P.E. Tsiakaras, V.A. Sobyanin, S.Y. Hramova, Solid State Ionics 152–153 (2002) 555–560.
[27] S. Assabumrungrat, W. Sangtongkitcharoen, N. Laosiripojana, A. Arpornwichanop, S. Charojrochkul, P. Praserthdam, J. Power Sources 148 (2005) 18–23.
[28] W. Jamsak, S. Assabumrungrat, P.L. Douglas, N. Laosiripojana, S. Charojrochkul, Chem. Eng. J. 119 (2006) 11–18.
[29] M. Ni, D.Y.C. Leung, M.K.H. Leung, J. Power Sources 183 (2008) 687–692.
[30] S.H. Chan, K.A. Khor, Z.T. Xia, J. Power Sources 93 (2001) 130–140.
[31] M. Ni, M.K.H. Leung, D.Y.C. Leung, Energy Convers. Manage. 48 (2007) 1525–1535.
[32] H.Y. Zhu, R.J. Kee, V.M. Janardhanan, O. Deutschmann, D.G. Goodwin, J. Electrochem. Soc. 152 (2005) A2427–A2440.
[33] M.C.J. Bradford, P.E. Fanning, M.A. Vannice, J. Catal. 172 (1997) 479–484.
[34] A. Skodra, M. Ouzounidou, M. Stoukides, Solid State Ionics 177 (2006) 2217–2220.
[35] C. Egawa, T. Nishida, S. Naito, K. Tamaru, J. Chem. Soc., Faraday Trans. 1 (1984) 1595–1604.
[36] A.S. Chellappa, C.M. Fisher, W.J. Thomson, Appl. Catal. A 227 (2002) 231–240.
[37] S.F. Yin, B.Q. Xu, X.P. Zhou, C.T. Au, Appl. Catal. A 277 (2004) 1–9.
[38] H.C. Liu, H. Wang, J.H. Shen, Y. Sun, Z.M. Liu, Appl. Catal. A 337 (2008) 138–147.
[39] W.Q. Zheng, J. Zhang, Q.J. Ge, H.Y. Xu, W.Z. Li, Appl. Catal. B 80 (2008) 98–105.
[40] T.V. Choudhary, C. Sivadinarayana, A. Klinghoffer, D.W. Goodman, Stud. Surf. Sci. Catal. 136 (2001) 197–202.
[41] J. Zhang, H.Y. Xu, X.L. Jin, Q.J. Ge, W.Z. Li, Appl. Catal. A 290 (2005) 87–96.
[42] S.F. Yin, Q.H. Zhang, B.Q. Xu, W.X. Zhu, C.F. Ng, C.T. Au, J. Catal. 224 (2004) 384–396.
[43] R. Suwanwarangkul, E. Croiset, M.W. Fowler, P.L. Douglas, E. Entchev, M.A. Douglas, J. Power Sources 122 (2003) 9–18.
[44] M. Ni, M.K.H. Leung, D.Y.C. Leung, J. Power Sources 168 (2007) 369–378.
[45] M. Ni, M.K.H. Leung, D.Y.C. Leung, Fuel Cells 7 (2007) 269–278.
[46] M. Ni, M.K.H. Leung, D.Y.C. Leung, Chem. Eng. Technol. 29 (2006) 636–642.
[47] M. Ni, M.K.H. Leung, D.Y.C. Leung, Electrochim. Acta 52 (2007) 6707–6718.
[48] R.C. Reid, J.M. Prausnitz, B.E. Poling, The Properties of Gases & Liquids, 4th ed., McGraw-Hill Book Company, New York, 1987.
[49] H.Y. Zhu, R.J. Kee, J. Power Sources 117 (2003) 61–74.
[50] R.R. Peng, Y. Wu, L.Z. Yang, Z.Q. Mao, Solid State Ionics 177 (2006) 389–393.
[51] M. Ni, D.Y.C. Leung, M.K.H. Leung, J. Power Sources 183 (2008) 133–142.